



HAL
open science

Resonant thermalization of periodically driven strongly correlated electrons

Francesco Peronaci, Marco Schiró, Olivier Parcollet

► **To cite this version:**

Francesco Peronaci, Marco Schiró, Olivier Parcollet. Resonant thermalization of periodically driven strongly correlated electrons. 2018. cea-01729411

HAL Id: cea-01729411

<https://cea.hal.science/cea-01729411>

Preprint submitted on 12 Mar 2018

HAL is a multi-disciplinary open access archive for the deposit and dissemination of scientific research documents, whether they are published or not. The documents may come from teaching and research institutions in France or abroad, or from public or private research centers.

L'archive ouverte pluridisciplinaire **HAL**, est destinée au dépôt et à la diffusion de documents scientifiques de niveau recherche, publiés ou non, émanant des établissements d'enseignement et de recherche français ou étrangers, des laboratoires publics ou privés.

Resonant thermalization of periodically driven strongly correlated electrons

Francesco Peronaci, Marco Schiró, and Olivier Parcollet

Institut de Physique Théorique (IPhT), CEA, CNRS, UMR 3681, 91191 Gif-sur-Yvette, France

(Dated: February 27, 2018)

We study the dynamics of the Fermi-Hubbard model driven by a time-periodic modulation of the interaction within nonequilibrium Dynamical Mean-Field Theory. For moderate interaction, we find clear evidence of thermalization to a genuine infinite-temperature state with no residual oscillations. Quite differently, in the strongly correlated regime, we find a quasi-stationary extremely long-lived state with oscillations synchronized with the drive (Floquet prethermalization). Remarkably, the nature of this state dramatically changes upon tuning the drive frequency. In particular, we show the existence of a critical frequency at which the system rapidly thermalizes despite the large interaction. We characterize this resonant thermalization and provide an analytical understanding in terms of a break down of the periodic Schrieffer-Wolff transformation.

Recent advances in the ability to tailor and control light-matter interaction on the ultra-fast time scale [1–4] have brought increasing interest in the manipulation of quantum phases of matter with periodic *driving* fields. Notable achievements are light-induced superconductivity [5, 6], metal-to-insulator transition [7] and control of microscopic parameters such as the local interaction in organic Mott insulators [8] and the band gap in excitonic insulators [9]. Similar ideas are applied to ultra-cold atoms in optical lattices [10] where driving fields are used, for instance, to engineer topological states [11].

From a theoretical perspective, periodically driven, or *Floquet*, quantum systems are a long-standing subject of studies ranging from dynamical localization [12] and quantum dissipation [13] to quantum chaos [14] and, more recently, isolated quantum many-body systems [15]. Other topics of active research include drive-induced topological states [16, 17] and artificial gauge fields [18]; driven electron-phonon coupling [19–21]; and integrable systems [22], correlated electrons [23–26] or topological systems [27, 28] in presence of dissipation.

In absence of integrability and of many-body localization, isolated out-of-equilibrium quantum many-body systems are expected to show thermalization of local observables at long times [29]. Driven systems, which lack time translational invariance, are therefore brought to *thermalize* to a featureless infinite-temperature state consistent with maximum entropy and no energy conservation [30–33]. Yet, the transient dynamics may leave space to non-trivial extremely long-lived non-thermal states characterized by oscillations synchronized with the drive, a phenomenon known as *Floquet prethermalization*. This prethermal behavior can emerge in the high frequency limit [34–40] or be the consequence of a nearby integrable point in the system parameter space. In this case, as recently observed for weakly [41–43] and strongly [44, 45] interacting systems, there are many quasi-integrals of motion that prevent thermalization except at very long times, similarly to what happens after a quantum quench [46]. However, many intriguing questions remain wide open especially concerning the inter-

mediate coupling and frequency regimes, where the most remarkable phenomena are expected to occur.

In this Letter we consider the Fermi-Hubbard model as paradigmatic example of strongly correlated electrons. The system is subject to a time-periodic modulation of the electron interaction, but it is otherwise isolated from any external reservoir. Starting from a thermal equilibrium state, we use non-equilibrium Dynamical Mean-Field Theory (DMFT) [47] to calculate the time evolution induced by the drive. First, we explicitly show that at moderate interaction the system thermalizes to the infinite-temperature state. Then, we turn to the regime of large interaction and find a long-lived prethermal state synchronized with the drive, except for a critical, resonant frequency where we find thermalization and a behavior reminiscent of a dynamical transition [48–50]. A periodic Schrieffer-Wolff transformation shows that the Floquet prethermalization is due to the quasi-conservation of double occupancy at large interaction, with the resonant thermalization emerging in correspondence of a break down of such an expansion.

The system is governed by the following Hamiltonian:

$$H(t) = \sum_{i,j} \sum_{\sigma=\uparrow,\downarrow} V_{ij} c_{i\sigma}^\dagger c_{j\sigma} + U(t) \sum_i (n_{i\uparrow} - \frac{1}{2})(n_{i\downarrow} - \frac{1}{2}), \quad (1)$$

where $U(t) = U_0 + \delta U \sin \Omega t$ is the periodically driven interaction and V_{ij} is the hopping, which is such that the bare density of states reads $\rho(\epsilon) = \sqrt{4V^2 - \epsilon^2}/(2\pi V^2)$ (Bethe lattice). We take V as unit of energy, frequency and inverse of time ($\hbar = 1$). In these units the bare band-width is $W = 4$ and the critical point of the Mott transition in DMFT is at $U_c \simeq 4.8$ and at an inverse temperature $\beta_c \simeq 20$. We consider a thermal initial density matrix $\rho(0) = \exp(-\beta H(0))$ with $\beta = 5$ and we fix the drive amplitude $\delta U = 2$ (cf. Supp. Mat. [51] Sec. ??). For all times the interaction remains repulsive and the system stays half-filled ($\langle n_\sigma \rangle = 0.5$) and particle-hole symmetric.

To calculate the time evolution induced by the drive we use nonequilibrium DMFT [47], which consists in map-

ping the lattice model described by Eq. (1) onto a quantum impurity problem with the following action:

$$\mathcal{S} = \mathcal{S}_{\text{loc}} + \int_{\mathcal{C}} dt dt' \sum_{\sigma=\uparrow,\downarrow} c_{\sigma}^{\dagger}(t) \Delta_{\sigma}(t, t') c_{\sigma}(t'), \quad (2)$$

where \mathcal{S}_{loc} is the action associated to the local term in Eq. (1), \mathcal{C} is the three branch Keldysh contour [52] and $\Delta_{\sigma}(t, t') = V^2 G_{\sigma}(t, t')$ is the hybridization between the impurity and a nonequilibrium bath, which is self-consistently determined from the impurity Green function $G_{\sigma}(t, t') = -i \langle T_{\mathcal{C}} c_{\sigma}(t) c_{\sigma}^{\dagger}(t') \rangle$. Within the DMFT mapping, the impurity Green function coincides with the local lattice Green function and from it we can calculate various quantities directly in the thermodynamic limit, such as the double occupancy $d(t) = \langle n_{i\uparrow}(t) n_{i\downarrow}(t) \rangle$ and the kinetic energy $K(t) = \sum_{ij\sigma} V_{ij} \langle c_{i\sigma}^{\dagger}(t) c_{j\sigma}(t) \rangle$. The computation of the impurity Green function is a challenging task and, despite recent progresses [53–55], an efficient and numerically exact approach is still lacking. Here we resort to the non-crossing approximation [56–63] which consists in a first order self-consistent hybridization expansion and which we implement through a Dyson equation for the impurity atomic-state propagator (cf. Supp. Mat. [51] Sec. ??). For moderate interaction, we benchmark the results with the next-order one-crossing approximation (cf. Supp. Mat. [51] Sec. ??).

We start by discussing the results for moderate average interaction $U_0 = 4$ (Fig. 1). The double occupancy shows fast oscillations with frequency comparable to the one of the drive Ω superimposed to a slower but exponential relaxation. Quite interestingly, after the initial transient and despite the continuous driving, the oscillations get fully damped and the double occupancy reaches the value $d_{\text{th}} = 0.25$ independently of the frequency. This is the value of a maximally disordered state and as such signals the thermalization to infinite temperature. With an exponential fit we can extract the thermalization time τ_{th} which is minimum for $\Omega \simeq 4.8$ and diverges for large frequency.

Thermalization is confirmed by the evolution of the Green function and in particular of the retarded component $G_{\sigma}^R(t, t') = -i\theta(t - t') \langle \{c_{\sigma}(t), c_{\sigma}^{\dagger}(t')\} \rangle$ and the lesser component $G_{\sigma}^<(t, t') = i \langle c_{\sigma}^{\dagger}(t') c_{\sigma}(t) \rangle$. In a thermal state these functions depend only on the difference $t - t' = \tau$ and their Fourier transform is related by the fluctuation-dissipation theorem. Out-of-equilibrium one can perform a Fourier transform with respect to τ at fixed $\bar{t} = (t + t')/2$ [64] and obtain the spectral function $A(\omega, \bar{t}) = -1/\pi \sum_{\sigma} \text{Im} G_{\sigma}^R(\omega, \bar{t})$ and the occupation function $N(\omega, \bar{t}) = i/(2\pi) \sum_{\sigma} G_{\sigma}^<(\omega, \bar{t})$. As a consequence of the time-dependent interaction, these functions have oscillations in \bar{t} with period $T = 2\pi/\Omega$ and are even negative for some ω . To extract meaningful information about the thermalization, which happens on times $\tau_{\text{th}} \gg T$, we average $A(\omega, \bar{t})$ and $N(\omega, \bar{t})$ over a few periods and obtain

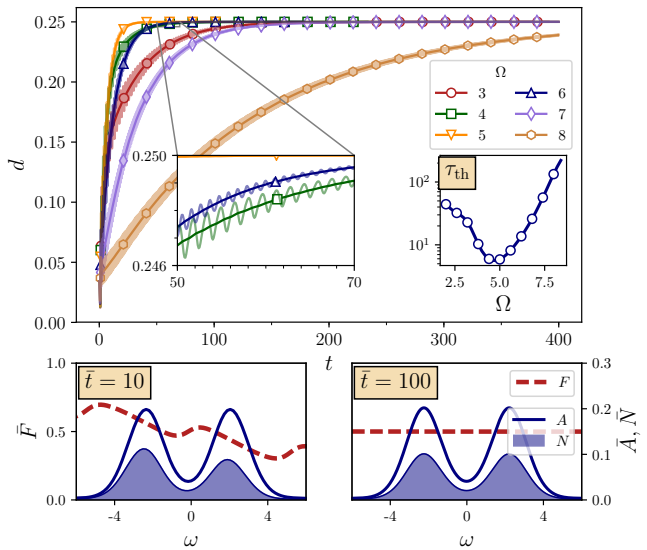


FIG. 1. Thermalization to infinite temperature ($U_0 = 4$). Top panel: Double occupancy $d(t)$ for various drive frequencies Ω shows oscillations (shade) on top of an exponential relaxation (solid line). Right inset: Thermalization time $\tau_{\text{th}}(\Omega)$. Bottom panels: Averaged spectral function $\bar{A}(\omega, \bar{t})$, occupation function $\bar{N}(\omega, \bar{t})$ and distribution function $\bar{F}(\omega, \bar{t}) = \bar{N}(\omega, \bar{t})/\bar{A}(\omega, \bar{t})$ for $\Omega = 4$ show the evolution from the out-of-equilibrium state at $\bar{t} = 10$ to the infinite-temperature thermal state at $\bar{t} = 100$.

positive $\bar{A}(\omega, \bar{t})$ and $\bar{N}(\omega, \bar{t})$ (cf. Supp. Mat. [51] Sec. ??). The distribution function $\bar{F}(\omega, \bar{t}) = \bar{N}(\omega, \bar{t})/\bar{A}(\omega, \bar{t})$ provides a simple indicator for thermalization since in the thermal state it equals the Fermi-Dirac distribution. In this case at early times we observe a non-thermal distribution with a pseudo-periodic structure in ω with period Ω . This feature is related to the so-called Floquet subbands characteristic of periodically driven systems [23]. Then, at later times we observe a remarkably flat distribution – clearly the only one to be at the same time thermal and pseudo-periodic. This establishes that the fluctuation-dissipation relation is satisfied with infinite temperature and therefore confirms thermalization.

We now turn to the strong coupling regime at large average interaction $U_0 = 8$ (Fig. 2). The transition from moderate interaction appears to be rather smooth (cf. Supp. Mat. [51] Sec. ??), however for large interaction, in contrast with above, we find qualitative differences as a function of the drive frequency. As a first indication, while for short times also in this case local observables oscillate on top of an exponential relaxation, now the stationary value depends on frequency. As we detail in the following, this signals the existence of different dynamical regimes. In particular, we find thermalization and damping of the oscillations only for a critical frequency, which we estimate to be $\Omega^* \simeq 8.12$, while for the other frequencies we observe a long-lived prethermal state.

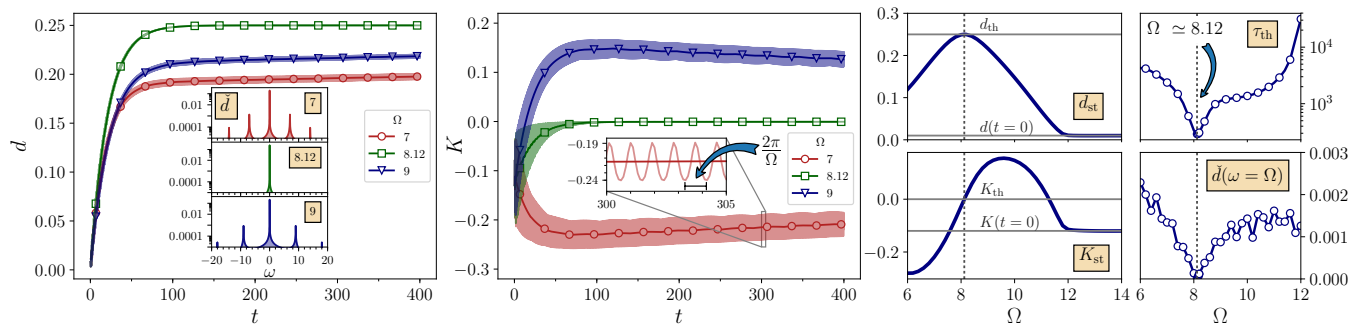


FIG. 2. Floquet prethermalization and resonant thermalization ($U_0 = 8$). Left panel: Double occupancy $d(t)$ for various drive frequencies Ω shows oscillations (shade) on top of an exponential relaxation (solid line). Central panel: same for kinetic energy. Inset of left panel: Fourier transform $\check{d}(\omega)$. Right panels: Top left: stationary value $d_{st}(\Omega)$ with thermal value d_{th} and initial value $d(t=0)$ for reference. Bottom left: same for kinetic energy. Top right: estimated thermalization time $\tau_{th}(\Omega)$. Bottom right: weight of the peak $\check{d}(\omega = \Omega)$. Dotted lines mark the resonant frequency $\Omega^* \simeq 8.12$. For $\Omega = 7, 9$ we see Floquet prethermalization with $d_{st} \neq d_{th}$, $K_{st} \neq K_{th}$ and \check{d} peaked at $\omega = \pm\Omega, \pm 2\Omega$. For $\Omega = \Omega^*$ not only $d_{st} = d_{th}$ and $K_{st} = K_{th}$ but also the sharp minimum of $\tau_{th}(\Omega)$ and the vanishing of $\check{d}(\omega = \Omega)$ signal the resonant thermalization.

For frequency below Ω^* the double occupancy and the kinetic energy oscillate around an average which relaxes exponentially to a non-thermal plateau after the initial transient. While for moderate interaction these oscillations damp out, here they persist with constant amplitude. We calculate the Fourier transform $\check{d}(\omega) = \int_{\tau_{pth}}^{t_{max}} dt e^{i\omega t} d(t)$ where τ_{pth} is the prethermalization time when the plateau is attained and t_{max} is the maximum simulation time. The peaks of \check{d} at multiples of Ω demonstrate the synchronization of the oscillations with the drive. This, together with the non-thermal value of the plateau, are the distinctive features of a Floquet prethermal state in which the system appears to be trapped for times longer than numerically accessible. Since the plateau has a slight linear positive slope, we can extrapolate it to intercept the thermal value $d_{th} = 0.25$ and in this way estimate a thermalization time τ_{th} which turns out to be orders of magnitude larger than at moderate interaction.

For frequency above Ω^* we find a very similar prethermalization regime until, for $\Omega \simeq U_0 + W = 12$, we observe a sharp threshold behavior. This value corresponds to the maximum energy for single-particle excitations above which the system appears to be unable to absorb energy and local observables are almost constant and equal to their initial equilibrium values. Accordingly, the thermalization time grows exponentially with frequency, in agreement with rigorous bounds [35, 39]. We remark also that, for a range of frequencies, the kinetic energy becomes positive, which is characteristic of a highly nonequilibrium state with population inversion. While a similar phenomenon is observed in other Floquet systems [24], here it cannot be ascribed to an effective change of sign of the interaction, since this would also cause the double occupancy to increase above 0.25.

The above picture radically changes for the critical fre-

quency $\Omega^* \simeq 8.12$ where fast thermalization is found despite the large interaction. Here we observe an exponential relaxation of the double occupancy and of the kinetic energy to the thermal values, together with a full damping of oscillations. At this specific frequency the Floquet prethermal state is therefore melted away and the system is able to relax to the infinite-temperature thermal state. We name this phenomenon *resonant* thermalization since for Ω^* the periodic modulation of the interaction is resonant with the energy $\sim U_0$ of doublon excitations, i.e. excitations that change the double occupancy. This resonant condition allows the absorption of energy from the drive and the creation of doublons, which are otherwise suppressed by the large average interaction through a well-known bottleneck mechanism [65, 66]. Remarkably, the behavior of the system around Ω^* is strongly reminiscent of a dynamical transition [48–50]. This is clearly seen in the estimated thermalization time $\tau_{th}(\Omega)$ which has a sharp minimum for Ω^* , as well as from the peak at $\omega = \Omega$ of the Fourier transform $\check{d}(\omega)$. The weight of this peak goes to zero for Ω^* with singular behavior, indicating the breakdown of synchronization and the approach to the stationary thermal value.

The above results are corroborated by the evolution of the spectral, occupation and distribution functions (Fig. 3). After the initial transient, these functions reach a stationary state independent of \bar{t} . This confirms that the plateau of the local observables corresponds to a true steady state of the system. For $\Omega \neq \Omega^*$ the distribution function $\bar{F}(\omega, \bar{t})$ is clearly non-thermal and pseudo- Ω -periodic, as also found for the non-thermal transient at moderate interaction. On the opposite, for the critical frequency Ω^* we find a remarkably flat distribution which confirms the thermalization at infinite temperature. Interestingly, for $\Omega > \Omega^*$, corresponding to positive kinetic energy, we indeed find a population inversion, as it is

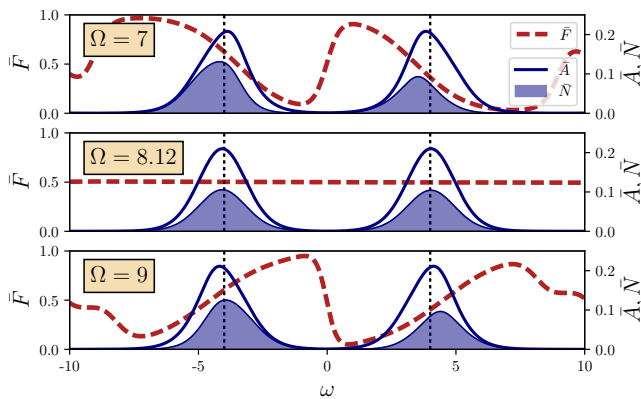


FIG. 3. Averaged spectral function $\bar{A}(\omega, \bar{t})$, occupation function $\bar{N}(\omega, \bar{t})$ and $\bar{F}(\omega, \bar{t}) = \bar{N}(\omega, \bar{t})/\bar{A}(\omega, \bar{t})$ for $U_0 = 8$ and $\bar{t} = 100$. Prethermalization for $\Omega = 7, 9$ and thermalization for $\Omega = \Omega^* \simeq 8.12$. For $\Omega = 9$ the population inversion is clear from the shift of \bar{N} towards higher energy and the change of slope of \bar{F} with respect to $\Omega = 7$. Dotted lines mark the approximate middle of the Hubbard bands.

clear from the shift towards high energy of \bar{N} and the change of slope of \bar{F} with respect to $\Omega < \Omega^*$.

To gain an analytical insight into the Floquet prethermalization and the resonant thermalization we use a Floquet Schrieffer-Wolff transformation [67–69]. This conveniently describes the strong coupling regime, where doublon excitations are suppressed because of the large average interaction, thus preventing the system from absorbing energy unless the frequency of the drive is resonant with the doublon energy. In practice, we introduce a time-periodic unitary $R(t) = \exp S(t)$ which eliminates perturbatively in V/U_0 the terms that do not conserve the double occupancy in the transformed Hamiltonian $\tilde{H} = e^S H e^{-S} - i\partial_t S$. This is obtained with an ansatz $S(t) = (V/U_0)(\alpha(t)K_+ - \alpha^*(t)K_-)$ where $\alpha(t)$ is a periodic function determined imposing the vanishing of the commutator $[\tilde{H}, \sum_i n_{i\uparrow}n_{i\downarrow}]$ up to terms of a given order in V/U_0 , and where we decompose the kinetic energy in terms that do not change (K_0), increase (K_+), or decrease (K_-) the double occupancy (cf. Supp. Mat. [51] Sec. ??). For generic drive frequency the transformation is well behaved and at first order in V/U_0 we find:

$$d(t) = d(0) - 2(V/U_0)\text{Re}[\alpha(T)\text{Tr}(\rho(0)K_+)] + 2(V/U_0)\text{Re}[\alpha(t)e^{i\int_0^t U(t')dt'}\text{Tr}(\rho(0)K_+(t))], \quad (3)$$

where $K_+(t) \equiv e^{iVK_0t}K_+e^{-iVK_0t}$. Eq. (3) captures the Floquet prethermal state at long times multiples of $T = 2\pi/\Omega$ (stroboscopic evolution) when the double occupancy is synchronized with the drive and oscillates around a frequency-dependent non-thermal value. However, for the critical value $\Omega^* \simeq U_0$ and its submultiples, the function α develops a singularity and the transformation breaks down. This suggests that, at these fre-

quencies, the Floquet prethermal state is unstable towards thermalization through non-perturbative processes in V/U_0 , as captured by DMFT. Calculations at large interaction $U_0 = 14$ and drive amplitude $\delta U = 6$ clearly show the resonant thermalization for frequencies Ω^* and $\Omega^*/2$ (cf. Supp. Mat. [51] Sec. ??).

The results we have presented here have a potential impact on various experiments, ranging from ultra-cold atoms in driven optical lattices, where one should observe a sudden increase of the heating rate [70] at $\Omega = \Omega^*$; to photo-excited organic Mott insulators [8], where one should observe a sudden filling of the gap in the transient optical conductivity. We also envisage further theoretical study, in particular on the effect of non-local correlations in realistic lattices, which are likely to affect the lifetime of the prethermal plateau. Advances in the solution of the impurity problem would also be important, as they would permit further investigations of the transition between moderate and large interaction and the access to initial states at lower temperature.

In conclusion, to study periodically driven strongly correlated electrons, we have considered the Fermi-Hubbard model with time-periodic interaction. Within nonequilibrium DMFT we have calculated the evolution of local observables and of the local Green function, which provide evidence for thermalization or prethermalization. We have showed the existence of three dynamical regimes: (i) Thermalization to infinite temperature at moderate interaction, as expected for generic isolated quantum many-body systems; (ii) Floquet prethermalization at large interaction, characterized by oscillations of local observables around a non-thermal plateau and a stationary non-thermal distribution function; (iii) Resonant thermalization at large interaction for an isolated critical frequency Ω^* , where local observables relax exponentially to the infinite-temperature thermal value, together with a damping of oscillations and a flat distribution function. We have then developed a periodic Schrieffer-Wolff transformation which captures the qualitative features of the Floquet prethermal state and whose breakdown for Ω^* indicates the non-perturbative nature of the resonant thermalization phenomenon.

This work is supported by the FP7/ERC, under Grant Agreement No. 278472-MottMetals. MS acknowledges support from a grant ‘‘Investissements d’Avenir’’ from LabEx PALM (ANR-10-LABX-0039-PALM) and from the CNRS through the PICS-USA-14750.

-
- [1] J. Orenstein, *Physics Today* **65**, 44 (2012).
 - [2] D. Nicoletti and A. Cavalleri, *Advances in Optics and Photonics* **8**, 401 (2016).
 - [3] M. Först, C. Manzoni, S. Kaiser, Y. Tomioka, Y. Tokura, R. Merlin, and A. Cavalleri, *Nature Physics* **7**, 854 (2011).

- [4] A. Subedi, A. Cavalleri, and A. Georges, *Physical Review B* **89**, 220301 (2014).
- [5] D. Fausti, R. I. Tobey, N. Dean, S. Kaiser, A. Dienst, M. C. Hoffmann, S. Pyon, T. Takayama, H. Takagi, and A. Cavalleri, *Science* **331**, 189 (2011).
- [6] M. Mitrano, A. Cantaluppi, D. Nicoletti, S. Kaiser, A. Perucchi, S. Lupi, P. Di Pietro, D. Pontiroli, M. Riccò, S. R. Clark, D. Jaksch, and A. Cavalleri, *Nature* **530**, 461 (2016).
- [7] G. Lantz, B. Mansart, D. Grieger, D. Boschetto, N. Nilforoushan, E. Papalazarou, N. Moisan, L. Perfetti, V. L. R. Jacques, D. Le Bolloc'h, C. Laulhé, S. Ravy, J.-P. Rueff, T. E. Glover, M. P. Hertlein, Z. Hussain, S. Song, M. Chollet, M. Fabrizio, and M. Marsi, *Nature Communications* **8**, 13917 (2017).
- [8] R. Singla, G. Cotugno, S. Kaiser, M. Först, M. Mitrano, H. Y. Liu, A. Cartella, C. Manzoni, H. Okamoto, T. Hasegawa, S. R. Clark, D. Jaksch, and A. Cavalleri, *Physical Review Letters* **115**, 187401 (2015).
- [9] S. Mor, M. Herzog, D. Golež, P. Werner, M. Eckstein, N. Katayama, M. Nohara, H. Takagi, T. Mizokawa, C. Monney, and J. Stähler, *Physical Review Letters* **119**, 086401 (2017).
- [10] I. Bloch, J. Dalibard, and W. Zwerger, *Reviews of Modern Physics* **80**, 885 (2008); I. Bloch, J. Dalibard, and S. Nascimbène, *Nature Physics* **8**, 267 (2012).
- [11] A. Eckardt, *Reviews of Modern Physics* **89**, 011004 (2017); G. Jotzu, M. Messer, R. Desbuquois, M. Lebrat, T. Uehlinger, D. Greif, and T. Esslinger, *Nature* **515**, 237 (2014).
- [12] D. H. Dunlap and V. M. Kenkre, *Physical Review B* **34**, 3625 (1986).
- [13] M. Grifoni and P. Hänggi, *Physics Reports* **304**, 229 (1998).
- [14] G. Casati and B. V. Chirikov, *Quantum chaos: Between order and disorder* (Cambridge University Press, 1995).
- [15] R. Moessner and S. L. Sondhi, *Nature Physics* **13**, 424 (2017).
- [16] T. Oka and H. Aoki, *Physical Review B* **79**, 081406 (2009).
- [17] N. H. Lindner, G. Refael, and V. Galitski, *Nature Physics* **7**, 490 (2010).
- [18] N. Goldman and J. Dalibard, *Physical Review X* **4**, 031027 (2014).
- [19] M. Knap, M. Babadi, G. Refael, I. Martin, and E. Demler, *Physical Review B* **94**, 214504 (2016).
- [20] M. Babadi, M. Knap, I. Martin, G. Refael, and E. Demler, *Physical Review B* **96**, 014512 (2017).
- [21] Y. Murakami, N. Tsuji, M. Eckstein, and P. Werner, *Physical Review B* **96**, 045125 (2017).
- [22] F. Lange, Z. Lenarčič, and A. Rosch, *Nature Communications* **8**, 15767 (2017).
- [23] N. Tsuji, T. Oka, and H. Aoki, *Physical Review B* **78**, 235124 (2008); *Physical Review Letters* **103**, 047403 (2009).
- [24] N. Tsuji, T. Oka, P. Werner, and H. Aoki, *Physical Review Letters* **106**, 236401 (2011).
- [25] J. R. Coulthard, S. R. Clark, S. Al-Assam, A. Cavalleri, and D. Jaksch, *Physical Review B* **96**, 085104 (2017).
- [26] G. Mazza and A. Georges, *Physical Review B* **96**, 064515 (2017).
- [27] H. Dehghani, T. Oka, and A. Mitra, *Physical Review B* **90**, 195429 (2014); *Physical Review B* **91**, 155422 (2015).
- [28] H. Dehghani and A. Mitra, *Physical Review B* **92**, 165111 (2015); *Physical Review B* **93**, 245416 (2016).
- [29] M. Rigol, V. Dunjko, and M. Olshanii, *Nature* **452**, 854 (2007).
- [30] L. D'Alessio and M. Rigol, *Physical Review X* **4**, 041048 (2014).
- [31] A. Lazarides, A. Das, and R. Moessner, *Physical Review Letters* **112**, 150401 (2014).
- [32] P. Ponte, A. Chandran, Z. Papić, and D. A. Abanin, *Annals of Physics* **353**, 196 (2015).
- [33] M. Genske and A. Rosch, *Physical Review A* **92**, 062108 (2015).
- [34] M. Bukov, L. D'Alessio, and A. Polkovnikov, *Advances in Physics* **64**, 139 (2015).
- [35] D. A. Abanin, W. De Roeck, and F. Huveneers, *Physical Review Letters* **115**, 256803 (2015).
- [36] T. Kuwahara, T. Mori, and K. Saito, *Annals of Physics* **367**, 96 (2016).
- [37] M. Bukov, M. Heyl, D. A. Huse, and A. Polkovnikov, *Physical Review B* **93**, 155132 (2016).
- [38] T. Mori, T. Kuwahara, and K. Saito, *Physical Review Letters* **116**, 120401 (2016).
- [39] D. A. Abanin, W. De Roeck, W. W. Ho, and F. Huveneers, *Physical Review B* **95**, 014112 (2017).
- [40] F. Machado, G. D. Meyer, D. V. Else, C. Nayak, and N. Y. Yao, *arXiv:1708.01620* (2017).
- [41] M. Bukov, S. Gopalakrishnan, M. Knap, and E. Demler, *Physical Review Letters* **115**, 205301 (2015).
- [42] E. Canovi, M. Kollar, and M. Eckstein, *Physical Review E* **93**, 012130 (2016).
- [43] S. A. Weidinger and M. Knap, *Scientific Reports* **7**, 45382 (2016).
- [44] K. I. Seetharam, P. Titum, M. Kolodrubetz, and G. Refael, *arXiv:1710.09843* (2017).
- [45] A. Herrmann, Y. Murakami, M. Eckstein, and P. Werner, *arXiv:1711.07241*, 1 (2017).
- [46] M. Moeckel and S. Kehrein, *Physical Review Letters* **100**, 175702 (2008).
- [47] H. Aoki, N. Tsuji, M. Eckstein, M. Kollar, T. Oka, and P. Werner, *Reviews of Modern Physics* **86**, 779 (2014).
- [48] M. Eckstein, M. Kollar, and P. Werner, *Physical Review Letters* **103**, 056403 (2009).
- [49] M. Schiró and M. Fabrizio, *Physical Review Letters* **105**, 076401 (2010).
- [50] N. Tsuji, M. Eckstein, and P. Werner, *Physical Review Letters* **110**, 136404 (2013).
- [51] See Supplemental Materials at ... for additional data with different interaction and drive amplitude, for details on the non-crossing and one-crossing approximations, the spectral analysis and the Schrieffer-Wolff transformation.
- [52] G. Stefanucci and R. van Leeuwen, *Nonequilibrium Many-Body Theory of Quantum Systems* (Cambridge University Press, Cambridge, 2013).
- [53] G. Cohen, E. Gull, D. R. Reichman, and A. J. Millis, *Physical Review Letters* **115**, 266802 (2015).
- [54] A. E. Antipov, Q. Dong, J. Kleinhenz, G. Cohen, and E. Gull, *Physical Review B* **95**, 085144 (2017).
- [55] R. E. V. Profumo, C. Groth, L. Messio, O. Parcollet, and X. Waintal, *Physical Review B* **91**, 245154 (2015).
- [56] N. E. Bickers, *Reviews of Modern Physics* **59**, 845 (1987).
- [57] P. Nordlander, M. Pustilnik, Y. Meir, N. S. Wingreen, and D. C. Langreth, *Physical Review Letters* **83**, 808 (1999).
- [58] A. Rüegg, E. Gull, G. A. Fiete, and A. J. Millis, *Physical Review B* **87**, 075124 (2013).

- [59] M. Eckstein and P. Werner, *Physical Review B* **82**, 115115 (2010).
- [60] M. Eckstein, T. Oka, and P. Werner, *Physical Review Letters* **105**, 146404 (2010).
- [61] M. Eckstein and P. Werner, *Physical Review B* **84**, 035122 (2011); *Physical Review Letters* **110**, 126401 (2013).
- [62] H. U. Strand, M. Eckstein, and P. Werner, *Physical Review X* **5**, 011038 (2015).
- [63] D. Golež, M. Eckstein, and P. Werner, *Physical Review B* **92**, 195123 (2015).
- [64] M. Eckstein and M. Kollar, *Physical Review B* **78**, 205119 (2008).
- [65] A. Rosch, D. Rasch, B. Binz, and M. Vojta, *Physical Review Letters* **101**, 265301 (2008).
- [66] R. Sensarma, D. Pekker, E. Altman, E. Demler, N. Strohmaier, D. Greif, R. Jördens, L. Tarruell, H. Moritz, and T. Esslinger, *Physical Review B* **82**, 224302 (2010).
- [67] J. R. Schrieffer and P. A. Wolff, *Physical Review* **149**, 491 (1966).
- [68] M. Bukov, M. Kolodrubetz, and A. Polkovnikov, *Physical Review Letters* **116**, 125301 (2016).
- [69] M. M. Wysokiński and M. Fabrizio, *Physical Review B* **96**, 201115 (2017).
- [70] M. Reitter, J. Näger, K. Wintersperger, C. Sträter, I. Bloch, A. Eckardt, and U. Schneider, *Physical Review Letters* **119**, 200402 (2017).

Supplemental Material for: Resonant thermalization of periodically driven strongly correlated electrons

Francesco Peronaci, Marco Schiró, and Olivier Parcollet
Institut de Physique Théorique (IPhT), CEA, CNRS, UMR 3681, 91191 Gif-sur-Yvette, France

The supplemental material is structured as follows. In Sec. I we present additional data and discuss the role of the drive amplitude and average interaction. In Sec. II we provide evidence for the thermalization at half the resonant frequency Ω^* . In Sec. III we give the equations of the non-crossing (NCA) and one-crossing (OCA) approximations and in Sec. IV we provide OCA benchmark data at moderate interaction. In Sec. V we explain the analysis of the spectral function. Finally, in Sec. VI we discuss the Floquet Schrieffer-Wolff transformation.

I. ROLE OF DRIVE AMPLITUDE AND AVERAGE INTERACTION

In the main text we have considered a driven interaction $U(t) = U_0 + \delta U \sin \Omega t$ with drive amplitude $\delta U = 2$ and average interaction $U_0 = 4$ and $U_0 = 8$. Here we provide data which clarify the role of these parameters. In Figure 1 we plot the time evolution of the double occupancy at fixed large interaction and different drive amplitudes. Quite interestingly, a larger drive amplitude has different effects for drive frequency far from resonance or close to resonance. In the former case ($\Omega = 5$) we observe that a large drive amplitude makes the system thermalize despite the large average interaction. As opposite, near resonance ($\Omega = 9$) we observe a faster dy-

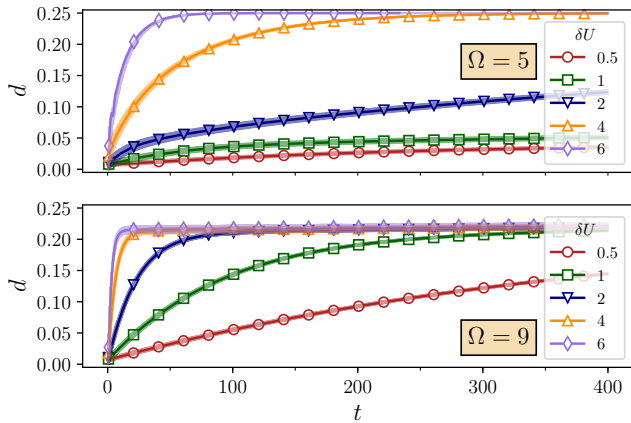


FIG. 1. Role of drive amplitude at average interaction $U_0 = 8$. Top panel: For drive frequency $\Omega = 5$, well below the resonance Ω^* , a larger amplitude makes the system to thermalize. Bottom panel: For frequency close to resonance ($\Omega = 9$) a larger amplitude gives a faster relaxation to the prethermal plateau, whose value does not depend on the drive amplitude.

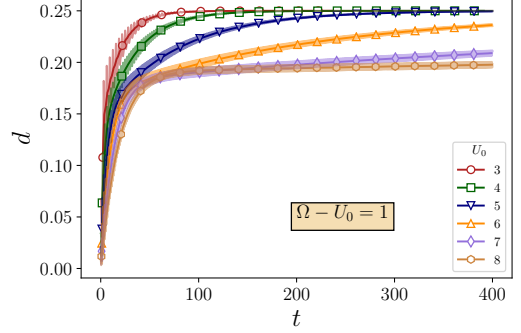


FIG. 2. Evolution from moderate to large interaction at fixed $\Omega - U_0 = 1$. A kink is visible at $\tau_{\text{pth}} \simeq 25$ for $U_0 = 5, 6$ at which the dynamics slows down.

namics which, however, eventually saturates to the same prethermal plateau described in the main text. Remarkably, the value of this plateau does not depend on the drive amplitude, as opposed to its strong dependence on the drive frequency, as discussed in the main text.

A second interesting question concerns the connection of the regimes at moderate and large interactions discussed in the main text. In Figure 2 we plot the time evolution of the double occupancy with different average interactions and at a fixed difference $U_0 - \Omega = 1$. In this way we can disentangle the effect of a different interaction from an effective decrease of the drive frequency. As the interaction is increased from $U_0 = 3$ to $U_0 = 8$, we observe a rather smooth change, with the appearance of a well visible kink at $\tau_{\text{pth}} \simeq 25$ ($U_0 = 5, 6$) at which the dynamics slows down, and which eventually turns to a prethermal plateau.

II. RESONANT THERMALIZATION AT $\Omega^*/2$

The Floquet Schrieffer-Wolff transformation used in the main text and further discussed below, shows that the Floquet prethermal state is unstable towards thermalization whenever the drive frequency is resonant with the doublon excitation energy Ω^* and its submultiples. This suggests that around frequencies $\frac{\Omega^*}{n}$ with n integer we should observe a phenomenon similar to what discussed in the main text around Ω^* .

To confirm this picture, we present data with large average interaction $U_0 = 14$ and drive amplitude $\delta U = 6$. With these values the two resonances at Ω^* and $\frac{\Omega^*}{2}$ are well separated and, importantly, the frequency $\frac{\Omega^*}{2}$ is still

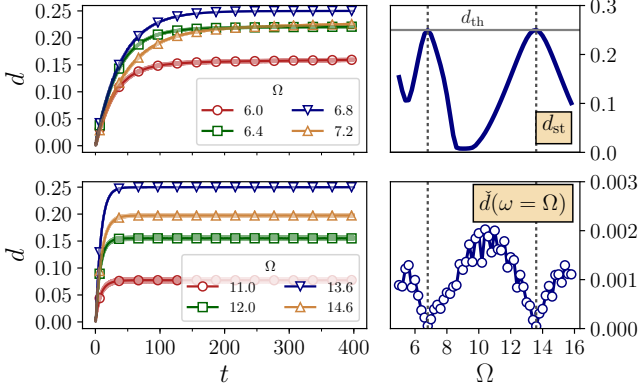


FIG. 3. Floquet prethermalization and resonant thermalization at $U_0 = 14$ and $\delta U = 6$. Left panels: double occupancy $d(t)$ shows a long-lived prethermal plateau eventually evolving to the thermal value as the frequency is swept across $\frac{\Omega^*}{2} \simeq 6.8$ (top) and $\Omega^* \simeq 13.6$ (bottom). Top right panel: stationary value $d_{\text{st}}(\Omega)$. Bottom right panel: weight of the Fourier component $\tilde{d}(\omega = \Omega)$ at the frequency of the drive.

reasonably high such that we can numerically access the time scale at which a prethermal plateau is well visible. In Figure 1 we provide evidence for the resonant thermalization at $\Omega^* \simeq 13.6$ and $\frac{\Omega^*}{2} \simeq 6.8$. Similarly to what discussed in the main text for $U_0 = 8$, the double occupancy relaxes to a prethermal plateau whose value is non-monotonic in the drive frequency. Around both Ω^* and $\frac{\Omega^*}{2}$ however, the double occupancy relaxes to the thermal value and, importantly, the amplitude of its oscillations vanishes. This second resonance is not observed at $U_0 = 8$ because in this case at $\frac{\Omega^*}{2} = 4$ the dynamics becomes much slower and a clear signature of prethermalization cannot be obtained within the numerically accessible time scales.

III. NON-CROSSING AND ONE-CROSSING APPROXIMATIONS

The non-crossing approximation (NCA) and one-crossing approximations (OCA) are based on the introduction of the atomic-state propagator R through the following Dyson equation:

$$i\partial_z R(z, z') = H_{\text{loc}}(z)R(z, z') + (S \otimes R)(z, z'), \quad (1a)$$

$$R(z, z^-) = -i\mathbb{1}, \quad (1b)$$

where $H_{\text{loc}}(z)$ is the local Hamiltonian and z, z' are variables on the three branch Keldysh contour \mathcal{C} , with z^- infinitesimally before z on \mathcal{C} .

In Eq. (1a) S is the self-energy of the atomic-state propagator, which describes the effects of the nonequilibrium bath on the dynamics of the impurity and can be expanded in powers of the hybridization Δ_σ . The NCA consists in a self-consistent truncation of this series at

the first order:

$$S^{(1)}(z, z') = i \sum_{\sigma=\uparrow, \downarrow} c_\sigma^\dagger R(z, z') c_\sigma \Delta_\sigma(z, z') - i \sum_{\sigma=\uparrow, \downarrow} c_\sigma R(z, z') c_\sigma^\dagger \Delta_\sigma(z', z), \quad (2)$$

while within the OCA one adds also the self-consistent second-order contributions:

$$S^{(2)}(z, z') = \sum_{\sigma'} \int_{z'}^z dz_1 \int_{z'}^{z_1} dz_2 \left[c_\sigma^\dagger R(z, z_1) c_{\sigma'}^\dagger R(z_1, z_2) c_\sigma R(z_2, z') c_{\sigma'} \Delta_\sigma(z, z_2) \Delta_{\sigma'}(z_1, z') - c_\sigma^\dagger R(z, z_1) c_{\sigma'} R(z_1, z_2) c_\sigma R(z_2, z') c_{\sigma'}^\dagger \Delta_\sigma(z, z_2) \Delta_{\sigma'}(z', z_1) - c_\sigma R(z, z_1) c_{\sigma'}^\dagger R(z_1, z_2) c_\sigma^\dagger R(z_2, z') c_{\sigma'} \Delta_\sigma(z_2, z) \Delta_{\sigma'}(z_1, z') + c_\sigma R(z, z_1) c_{\sigma'} R(z_1, z_2) c_\sigma^\dagger R(z_2, z') c_{\sigma'}^\dagger \Delta_\sigma(z_2, z) \Delta_{\sigma'}(z', z_1) \right]. \quad (3)$$

In Eq. (1a) it appears the following *clockwise* contour convolution:

$$(A \otimes B)(z, z') = \begin{cases} \int_{z'}^z d\bar{z} A(z, \bar{z}) B(\bar{z}, z') & \text{if } z > z', \\ \int_{0^+}^z d\bar{z} A(z, \bar{z}) B(\bar{z}, z') \\ + \int_{z'}^{-i\beta} d\bar{z} A(z, \bar{z}) B(\bar{z}, z') & \text{if } z < z', \end{cases} \quad (4)$$

where 0^+ and $-i\beta$ are, respectively, the first and last point of \mathcal{C} . Moreover it should be stressed that in Eqs. (1a) and (2) the products among R , H_{loc} , S , c_σ and c_σ^\dagger are to be understood as matrix products in the impurity Hilbert space. Since S depends on R in practice one has to solve iteratively Eqs. (1a) and (2) until a self-consistent solution is found. Moreover, this guarantees that the NCA and OCA are conserving approximations.

From the atomic-state propagator R we can calculate all the thermodynamics quantities of the impurity:

$$Z = \text{Tr}(iR(-i\beta, 0^+)), \quad (5)$$

$$n_\sigma(z) = \text{Tr}(\xi iR(z^-, z) c_\sigma^\dagger c_\sigma) Z^{-1}, \quad (6)$$

$$d(z) = \text{Tr}(\xi iR(z^-, z) c_\uparrow^\dagger c_\uparrow c_\downarrow^\dagger c_\downarrow) Z^{-1}, \quad (7)$$

where the trace is over the impurity Hilbert space, and $\xi_{mn} = \langle m | \xi | n \rangle = \pm \delta_{mn}$ if $|m\rangle$ contains an even or odd number of fermions. The equation for the Green function depends on the approximation used and within the NCA reads:

$$G_\sigma^{(1)}(z, z') = i \text{Tr}(\xi R(z', z) c_\sigma R(z, z') c_\sigma^\dagger) Z^{-1}, \quad (8)$$

while within the OCA one adds also the terms:

$$G_\sigma^{(2)}(z, z') = Z^{-1} \sum_{\sigma'} \int_z^{z'} dz_1 \int_{z'}^z dz_2 \left[\Delta(z_1, z_2) \text{Tr}(\xi R(z', z_1) c_{\sigma'}^\dagger R(z_1, z) c_\sigma R(z, z_2) c_{\sigma'} R(z_2, z') c_{\sigma'}^\dagger) - \Delta(z_2, z_1) \text{Tr}(\xi R(z', z_1) c_{\sigma'} R(z_1, z) c_\sigma R(z, z_2) c_{\sigma'}^\dagger R(z_2, z') c_{\sigma'}^\dagger) \right]. \quad (9)$$

The first step of the implementation is the projection of the various equations onto a basis of the impurity Hilbert space. In this case we can conveniently use the basis $\{|m\rangle\} = \{|0\rangle, |\uparrow\rangle, |\downarrow\rangle, |\uparrow\downarrow\rangle\}$ on which R , H_{loc} and S are diagonal. The second step is the projection of the equations onto the different Keldysh components, which can be made by means of the following Langreth rules for the clockwise convolution Eq. (4):

$$(A \otimes B)^>(t, t') = \int_{t'}^t d\bar{t} A^>(t, \bar{t}) B^>(\bar{t}, t'), \quad (10a)$$

$$(A \otimes B)^-(t, \tau) = \int_0^t d\bar{t} A^>(t, \bar{t}) B^-(\bar{t}, \tau) + \int_{\tau}^{\beta} d\bar{\tau} A^-(t, \bar{\tau}) B^M(\bar{\tau} - \tau), \quad (10b)$$

$$(A \otimes B)^<(t, t') = \int_0^t d\bar{t} A^>(t, \bar{t}) B^<(\bar{t}, t') - \int_0^{t'} d\bar{t} A^<(t, \bar{t}) B^>(\bar{t}, t') - i \int_0^{\beta} d\bar{\tau} A^-(t, \bar{\tau}) B^-(\bar{\tau}, t'), \quad (10c)$$

$$(A \otimes B)^M(\tau) = \int_0^{\tau} d\bar{\tau} A^M(\tau - \bar{\tau}) B^M(\bar{\tau}), \quad (10d)$$

which differ with respect to the rules for the usual convolution in two aspects: (i) the kernel in Eqs. (10a) to (10c) is the greater component instead of the retarded; (ii) the τ -integrals in Eqs. (10b) and (10d) are over a limited imaginary-time interval.

Importantly, under hermitian conjugation R satisfies the same properties of a bosonic or fermionic Green function:

$$(R^{\gtrless}(t, t'))^{\dagger} = -R^{\gtrless}(t', t), \quad (11)$$

$$(R^-(t, \tau))^{\dagger} = -\xi R^-(\beta - \tau, t), \quad (12)$$

and this can be used to restrict the calculation to half of the (t, t') plane and to get R^- from R^+ .

Finally, one needs the initial condition for the atomic-state propagator, which is obtained from R^M – whose equation is uncoupled from the other Keldysh components – through the following relations:

$$R^>(0, 0) = -i\mathbb{1}, \quad (13a)$$

$$R^<(0, 0) = i\xi R^M(\beta), \quad (13b)$$

$$R^-(0, \tau) = i\xi R^M(\beta - \tau). \quad (13c)$$

IV. OCA BENCHMARK AT MODERATE INTERACTION

We have performed benchmark calculations at moderate interaction $U_0 = 4$. In Figure 4 we plot the time evolution of the double occupancy for three different frequencies $\Omega = 3, 5, 7$ showing that the OCA corrections

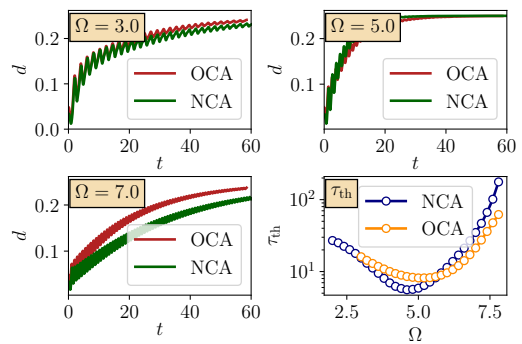


FIG. 4. Comparison NCA-OCA at moderate interaction $U_0 = 4$ and drive amplitude $\delta U = 2$. Top left, top right and bottom left panels: double occupancy $d(t)$ for different drive frequency and within OCA and NCA. Bottom right panel: thermalization time $\tau_{\text{th}}(\Omega)$ for OCA and NCA.

are only quantitative and, importantly, also in this case we observe thermalization. In the same figure, we compare the thermalization times within NCA and OCA, as extracted with an exponential fit of the time evolution. The OCA results thus shows the same qualitative features of the NCA, and slight quantitative differences such as a shift of the frequency at which the thermalization time τ_{th} is minimum from $\simeq 4.8$ to $\simeq 5.5$.

V. SPECTRAL FUNCTION ANALYSIS

Let us consider the retarded component of the Green function:

$$G_{\sigma}^R(t, t') = -i\theta(t - t') \langle \{c_{\sigma}(t), c_{\sigma}^{\dagger}(t')\} \rangle, \quad (14)$$

from which we calculate the time evolution of the spectral function discussed in the main text. The same analysis was carried out for the lesser component to derive the time evolution of the occupation function. In a thermal state $G_{\sigma}^R(t, t')$ depends only on the difference $t - t' = \tau$. Out-of-equilibrium one can perform a Fourier transform with respect to τ at fixed $\bar{t} = (t + t')/2$:

$$A(\omega, \bar{t}) = -\frac{1}{\pi} \sum_{\sigma} \text{Im} \int d\tau e^{i\omega\tau} G_{\sigma}^R(\bar{t} + \frac{\tau}{2}, \bar{t} - \frac{\tau}{2}). \quad (15)$$

As a consequence of the time-dependent interaction, this function has oscillations in \bar{t} with period $T = 2\pi/\Omega$ and is even negative for some ω . However we can average it over a few periods: $\bar{A}(\omega, \bar{t}) = 1/(nT) \int_{\bar{t}}^{\bar{t}+nT} A(\omega, \bar{t}') d\bar{t}'$ and obtain a positive spectral function (Fig. 5).

VI. FLOQUET SCHRIEFFER-WOLFF TRANSFORMATION

To derive the Floquet Schrieffer-Wolff transformation it is convenient to rewrite the Hamiltonian Eq. (1) of the

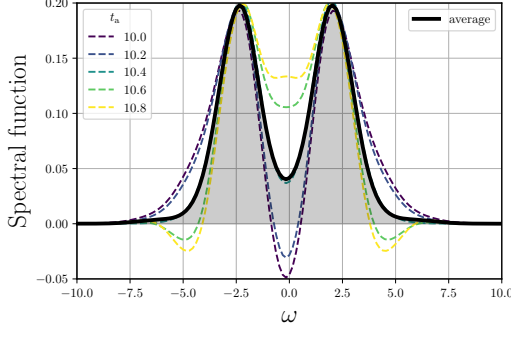


FIG. 5. Spectral function $\bar{A}(\omega, \bar{t})$ for $U_0 = 4$, $\delta U = 2$ and $\Omega = 4$ for different \bar{t} (dashed lines) and average over $n = 5$ periods (solid line).

main text as:

$$H(t) = U(t)D - V(K_0 + K_+ + K_-), \quad (16)$$

with the definition of the following operators:

$$D = \sum_i (n_{i\uparrow} - \frac{1}{2})(n_{i\downarrow} - \frac{1}{2}), \quad (17a)$$

$$K_0 = \sum_{\langle ij \rangle \sigma} c_{i\sigma}^\dagger c_{j\sigma} (n_{i\bar{\sigma}} n_{j\bar{\sigma}} + (1 - n_{i\bar{\sigma}})(1 - n_{j\bar{\sigma}})), \quad (17b)$$

$$K_+ = (K_-)^\dagger = \sum_{\langle ij \rangle \sigma} c_{i\sigma}^\dagger c_{j\sigma} n_{i\bar{\sigma}} (1 - n_{j\bar{\sigma}}), \quad (17c)$$

where with $\langle ij \rangle$ we indicate nearest-neighbor sites for which $V_{ij} = -V$. The double occupancy then reads $d(t) = \text{Tr} \rho(t) D$ and we have decomposed the kinetic energy in terms that do not change the double occupancy (K_0), increase it (K_+) or decrease it (K_-), as it is clear from the following commutators:

$$[D, K_0] = 0, \quad [D, K_\pm] = \pm K_\pm. \quad (18)$$

In the limit $V/U_0 = 0$ the double occupancy is a conserved quantity. To calculate the corrections in the case of small but finite V/U_0 we perform a change of basis:

$$\begin{aligned} \bar{\rho}(t) &\equiv R(t)\rho(t)R^\dagger(t) \\ &= R(t)U(t)\rho(0)U^\dagger(t)R^\dagger(t) \\ &= R(t)U(t)R^\dagger(0)\bar{\rho}(0)R(0)U^\dagger(t)R^\dagger(t) \\ &= \bar{U}(t)\bar{\rho}(0)\bar{U}^\dagger(t), \end{aligned} \quad (19)$$

where $U(t)$ and $\bar{U}(t) = R(t)U(t)R^\dagger(0)$ are the evolution operators in the original and in the new basis and:

$$i\partial_t \bar{U}_t = \tilde{H}(t)\bar{U}(t) \quad (20)$$

$$\begin{aligned} \tilde{H}(t) &= R(t)H(t)R^\dagger(t) - iR(t)\partial_t R^\dagger(t) \\ &= e^{-S(t)}H(t)e^{S(t)} - i\partial_t S(t) \end{aligned} \quad (21)$$

where we introduce the representation $R(t) = e^{-S(t)}$ with $S^\dagger(t) = -S(t)$. We can choose $S(t)$ in such a way to

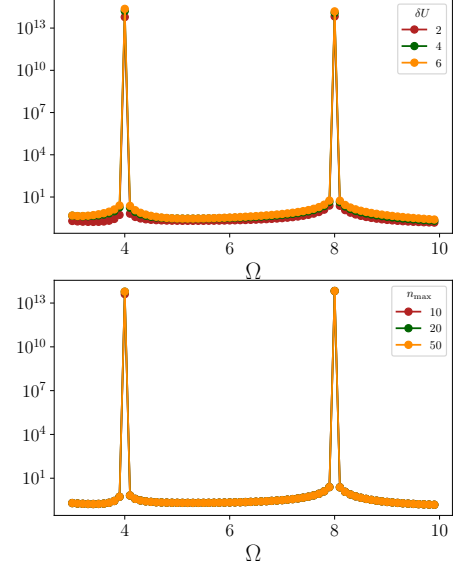


FIG. 6. Break down of the Schrieffer-Wolff transform. Plot of $|\sum_n \alpha_n|$ as a function of the frequency of the drive Ω for $U_0 = 8$ and for different δU (top panel, fixed $n_{\max} = 50$) or different n_{\max} (bottom panel, fixed $\delta U = 2$).

eliminate perturbatively in V/U_0 the terms in $\tilde{H}(t)$ that do not commute with D :

$$\begin{aligned} \tilde{H}(t) &= H(t) + [H(t), S(t)] - i\partial_t S(t) + \mathcal{O}(V^2/U_0) \\ &= U(t)D - V(K_0 + K_+ + K_-) \\ &\quad + U(t)[D, S(t)] - i\partial_t S(t) + \mathcal{O}(V^2/U_0). \end{aligned} \quad (22)$$

Therefore at first order we find the condition:

$$-V(K_+ + K_-) + U(t)[D, S(t)] - i\partial_t S(t) = 0. \quad (23)$$

If we now make a periodic ansatz of the following form inspired by the standard Schrieffer-Wolff transformation:

$$S(t) = \frac{V}{U_0} \sum_n e^{-in\Omega t} (\alpha_n K_+ - \alpha_{-n}^* K_-), \quad (24)$$

then the condition Eq. (23) becomes:

$$-U_0 \delta_{n,0} + \sum_m U_{n-m} \alpha_m - n\Omega \alpha_n = 0, \quad (25)$$

where U_n is the Fourier component of $U(t)$ and in particular if $U(t) = U_0 + \delta U \sin(\Omega t)$ we obtain:

$$(n\Omega - U_0)\alpha_n + i\frac{\delta U}{2}(\alpha_{n+1} - \alpha_{n-1}) = U_0 \delta_{n,0}. \quad (26)$$

If the system Eq. (26) is not singular, we can finally calculate the correction of order V/U_0 to the double occupancy:

$$\begin{aligned} d(t) &= \text{Tr}[R(0)\rho(0)R^\dagger(0)\bar{U}^\dagger(t)R(t)DR^\dagger(t)\bar{U}(t)] \\ &= \text{Tr}[\bar{\rho}(0)\bar{U}^\dagger(t)D\bar{U}(t)] \\ &\quad + \text{Tr}[\rho(0), S(0)]\bar{U}^\dagger(t)D\bar{U}(t) \\ &\quad + \text{Tr}[\rho(0)\bar{U}^\dagger(t)[D, S(t)]\bar{U}(t)]. \end{aligned} \quad (27)$$

which coincides term by term with Eq. (3) of the main text.

On the other hand, if the matrix A_{nm} is singular the above calculation breaks down. We have solved numerically this problem with a cut-off to the matrix size and

we show in Fig. 6 that this break down happens for a frequency of the drive $\Omega \simeq \frac{U_0}{n}$ with integer n . For this frequencies, despite the small V/U_0 , the corrections to a constant double occupancy are non-perturbative in V/U_0 and this explains why the system does not reach a prethermal plateau but instead is able to thermalize.